Received: 15 November 2023 | Revised: 27 February 2024 | Accepted: 28 February 2024

DOI: 10.1002/alz.13806

Alzheimer's & Dementia®
THE JOURNAL OF THE ALZHEIMER'S ASSOCIATION

RESEARCH ARTICLE

Early molecular events of autosomal-dominant Alzheimer's disease in marmosets with PSEN1 mutations

Gregg E. Homanics[1,2] | Jung Eun Park[2] | Lauren Bailey[3] | David J. Schaeffer[2] | Lauren Schaeffer[2] | Jie He[4] | Shuoran Li[4] | Tingting Zhang[4] | Annat Haber[5] | Catrina Spruce[5] | Anna Greenwood[6] | Takeshi Murai[3] | Laura Schultz[3] | Lauren Mongeau[3] | Seung-Kwon Ha[2] | Julia Oluoch[2] | Brianne Stein[2] | Sang Ho Choi[2] | Hasi Huhe[3] | Amantha Thathiah[2] | Peter L. Strick[2] | Gregory W. Carter[5] | Afonso C. Silva[2] | Stacey J. Sukoff Rizzo[2,3]

[1]Department of Anesthesiology & Perioperative Medicine, University of Pittsburgh School of Medicine, Pittsburgh, Pennsylvania, USA

[2]Department of Neurobiology, University of Pittsburgh Brain Institute, University of Pittsburgh School of Medicine, Pittsburgh, Pennsylvania, USA

[3]Department of Medicine, University of Pittsburgh Aging Institute, University of Pittsburgh School of Medicine, Pittsburgh, Pennsylvania, USA

[4]Department of Statistics, University of Pittsburgh School of Medicine, Pittsburgh, Pennsylvania, USA

[5]The Jackson Laboratory, Bar Harbor, Maine, USA

[6]Sage Bionetworks, Seattle, Washington, USA

Correspondence
Stacey J. Sukoff Rizzo, Department of Neurobiology, University of Pittsburgh School of Medicine, 514A Bridgeside Point I, 100 Technology Drive, Pittsburgh, PA 15219, USA.
Email: rizzos@pitt.edu

Gregg E. Homanics, Jung Eun Park, and Lauren Bailey are co-first authors.

Funding information
National Institutes of Health; NIA, Grant/Award Number: U19AG074866; University of Pittsburgh Medical Center, Grant/Award Number: IPA 2019 No. 16

Abstract

INTRODUCTION: Fundamental questions remain about the key mechanisms that initiate Alzheimer's disease (AD) and the factors that promote its progression. Here we report the successful generation of the first genetically engineered marmosets that carry knock-in (KI) point mutations in the presenilin 1 (*PSEN1*) gene that can be studied from birth throughout lifespan.

METHODS: CRISPR/Cas9 was used to generate marmosets with C410Y or A426P point mutations in *PSEN1*. Founders and their germline offspring are comprehensively studied longitudinally using non-invasive measures including behavior, biomarkers, neuroimaging, and multiomics signatures.

RESULTS: Prior to adulthood, increases in plasma amyloid beta were observed in PSEN1 mutation carriers relative to non-carriers. Analysis of brain revealed alterations in several enzyme–substrate interactions within the gamma secretase complex prior to adulthood.

DISCUSSION: Marmosets carrying KI point mutations in *PSEN1* provide the opportunity to study the earliest primate-specific mechanisms that contribute to the molecular and cellular root causes of AD onset and progression.

KEYWORDS
Alzheimer's disease, biomarkers, genetic engineering, marmosets, PSEN1

Highlights

- We report the successful generation of genetically engineered marmosets harboring knock-in point mutations in the PSEN1 gene.
- PSEN1 marmosets and their germline offspring recapitulate the early emergence of AD-related biomarkers.
- Studies as early in life as possible in PSEN1 marmosets will enable the identification of primate-specific mechanisms that drive disease progression.

1 | INTRODUCTION

Autosomal-dominant Alzheimer's disease (ADAD) results in an early-onset form of AD (EOAD), caused by mutations in either of three genes: amyloid precursor protein (*APP*), presenilin 1 (*PSEN1*), or presenilin 2 (*PSEN2*).[1–3] *PSEN1* mutations are the most common EOAD cases, accounting for approximately 80% of patients with nearly 100% penetrance before age 60.[4,5] Studies of patients with *PSEN1* mutations have provided vital insights into understanding the trajectory of AD progression including the timing of pathologic changes.[6–8] Data from several groups have now converged on a number of well-established findings: (1) there is a lengthy pre-symptomatic phase in ADAD mutation carriers that can be detected by biomarkers inclusive of blood, cerebrospinal fluid (CSF), and neuroimaging years before diagnosis and (2) the sequence of preclinical changes including elevated concentrations of Aβ1-42 in the plasma and CSF early in the pre-symptomatic phase is subsequent to the beginning of aggregation and accumulation in the brain as plaques.[5–18] Together these studies implicate evidence for events that emerge well before Aβ plaque deposition and, notably, prior to adulthood both in EOAD and late onset AD (LOAD).[15–17]

It is now clear that studies as early in life as possible in those with genetic risk for AD will be critical for identifying mechanisms that precede the cascade of known biochemical events in order to prevent disease inception.[19,20] A major challenge is the ability to obtain brain cells from living subjects from birth through the course of their life span in order to reveal changes that may be driving disease pathogenesis at the molecular and cellular levels. Therefore, animal models that recapitulate the natural onset and progression of the human disease can address many of the fundamental questions that remain about the key mechanisms that initiate the disease and the factors that promote its progression. Here we report the use of genetic engineering to create a model of ADAD in the marmoset, a small New World non-human primate (NHP). We selected the marmoset because its central nervous system shares many of the features that characterize the human brain, it breeds well in captivity, its life span is appropriate for the proposed experiments, and it displays age-related changes in brain structure and function that mirror those seen in humans.[21–23] Of particular relevance as a model for AD, Aβ deposits and hyperphosphorylated Tau aggregates occur spontaneously in the brain of aging marmosets, which does not naturally occur in rodent models of AD.[21–30]

The goal of these studies was to genetically engineer, in marmosets, the same knock-in (KI) point mutations of ADAD risk genes that confer EOAD in humans. The choice of mutation was inspired, in part, by studies of carriers of *PSEN1* C410Y and A426P mutations enrolled in a longitudinal study at the University of Pittsburgh.[31] We hypothesized that these specific KI mutations in marmosets would recapitulate the essential features of EOAD seen in humans with these *PSEN1* mutations, including the early hallmarks of overproduction of Aβ42 in plasma before cognitive decline.[5–18,31] Here, we report that marmosets with *PSEN1* KI point mutations display this hallmark of EOAD, and this phenotype is conserved in their germline offspring, consistent with ADAD mutations in humans. These marmosets are being comprehensively studied as part of the National Institute on Aging (NIA)-funded Marmosets as Research Models for Alzheimer's Disease (MARMO-AD) Consortium, which aims to bridge the rodent-to-human translational gap to identify primate-specific mechanisms that drive AD pathogenesis.[21] Importantly, the comprehensive study of these founder marmosets and their germline offspring longitudinally from birth throughout their lifespan will provide fundamental knowledge in our understanding of the biological processes that precede the known cascade of events and will enable the discovery of mechanisms that underlie AD inception and pathogenesis, as well as serving as model systems for evaluating interventions that have the potential to stop and prevent the onset of disease.

2 | METHODS

2.1 | Subjects

All animal experimental procedures were conducted in accordance with state and federal laws and locally approved by the University of Pittsburgh Institutional Animal Care and Use Committee (IACUC), and they were in line with and strictly adhered to the Guide for the Care and Use of Laboratory Animals.[32] Genetically diverse male and female

common marmosets (*Callithrix jacchus*) were enrolled in this study. Subjects were housed in an Association for Assessment and Accreditation of Laboratory Animal Care International (AAALAC)-accredited facility at the University of Pittsburgh and maintained at a temperature range of 76 to 78°F and 30% to 70% humidity, with a 12 h:12 h light/dark cycle (lights on at 7 a.m.). Subjects were fed a diet consisting of twice daily provision of commercial chow (Callitrichid High Fiber Diet #5LK7, Lab Diet; Marmoset Diet TD#130059, Envigo Teklad, Madison, WI, USA), supplemented with fresh fruit and vegetables daily with drinking water provided ad libitum. Foraging materials and enrichment were also provided daily. For each subject carrying the targeted mutation enrolled in the study, an age- and sex-matched contemporaneous non-carrier (NC) control best matched for litter size and birthweight was designated as the direct comparator for all procedures. All experiments were planned as life span studies unless welfare concerns deemed humane euthanasia necessary under the direction of a veterinarian. In the case of euthanasia, subjects were sedated with either an intramuscular injection of ketamine hydrochloride (Covetrus, Portland, ME, USA) or masked with isoflurane (Patterson Vet Supply Inc., Loveland, CO, USA), followed by an overdose of pentobarbital sodium (Covetrus, Portland, ME, USA). A transcardial perfusion with cold RNase-free phosphate buffered saline (PBS) was then performed. The brain was removed and separated into hemispheres, with the left hemisphere flash frozen using cold isopentane and stored at −135°C, while the right hemisphere and other peripheral tissues were placed in 10% neutral buffered formalin (NBF; Sigma-Aldrich) and stored at room temperature for histopathology.

RESEARCH IN CONTEXT

1. Systematic review: Using traditional sources (eg, PubMed, conference abstracts) the authors searched for studies describing the validation of non-human primate (NHP) models for translational studies of AD.
2. Interpretation: While studies have documented the natural occurrence of AD-related pathology in aged NHPs and the successful generation of genetically engineered marmosets with AD risk mutations, their clinical significance in the context of AD have not been comprehensively evaluated. We report the successful generation of genetically engineered marmosets harboring knock-in point mutations in the *PSEN1* gene that causes EOAD and the emergence of disease-related biomarkers before adolescence.
3. Future directions: Marmosets are an ideal NHP model for investigating the earliest primate-specific cellular and molecular events that lead to AD. The comprehensive study of gene-edited marmoset AD models from neurodevelopment through aging will identify emerging phenotypes that precede frank neuropathology. These animals will be invaluable resources for translational studies.

2.2 | Genetic engineering of *PSEN1* KI point mutations

We used Benchling.com to select guide RNAs (gRNAs) that uniquely bind to the marmoset genome near the KI substitution sites in the *PSEN1* gene (Figure 1A,B). The selected gRNA target sites were used to synthesize site-specific Alt-R CRISPR-Cas9 crRNAs (IDT DNA, Coralville, IA, USA), which were individually hybridized to a universal 67mer Alt-R CRISPR-Cas9 tracrRNA (IDT DNA) to produce gRNAs. The repair templates consisted of PAGE-purified Ultramer single-stranded DNA Oligos (IDT DNA) that were 120 nt long, with three phosphorothioate modifications on each end,[33] and were homologous to the target loci and harbored the desired KI mutations. Oocytes were collected by laparoscopic follicular aspiration from ovarian-stimulated donor females, as previously described.[34] Briefly, healthy female marmosets were selected as oocyte donors for superovulation, which was performed by intramuscular injection with human follitrophin alfa (human follicle stimulating hormone (FSH); Gonal-f, Merck Serono) for 8 days, then human chorionic gonadotropin (hCG; Chorulon, Merck Serono) on the ninth day. Oocytes were then sorted, matured, and fertilized in vitro, similarly to previous descriptions.[34] Briefly, in vitro oocyte maturation was performed by incubation in porcine oocyte medium (POM; Cosmo Bio Co. Ltd., Carlsbad, CA, USA) supplemented with 5% fetal bovine serum (Invitrogen, Carlsbad, CA, USA), 5 IU/mL FSH (Gonal-f, EMD Serono, Rockland, MA, USA), and 5 IU/mL hCG (Chorulon, Merck Serono) under mineral oil at 38°C in a humidified 5% CO_2, 5% O_2, and 90% N2. Matured oocytes were inseminated in vitro with motile spermatozoa obtained by sperm swim-up preparation of fresh ejaculate in Tyrode's albumin lactate pyruvate (TALP) medium (Caisson Labs, North Logan, UT, USA). The fertilized embryos were cultured in Cleav medium (Origio, Denmark) under mineral oil at 37°C in a humidified 5% CO_2, 5% O_2, and 90% N2. We injected the cytoplasm of single-cell embryos presenting two pronuclei with IDT Alt-R HiFi Cas9 Nuclease V3 protein (50 to 100 ng/μL), gRNA (25 to 50 ng/μL), and repair template (50 to 100 ng/μL). Embryos that survived microinjection were cultured for ~3 days in Cleav (Origio). Those that developed to the 8+ cell stage were non-surgically transferred transcervically to the uterus of synchronized recipients (—two to four embryos/recipient) as described.[35] Pregnancies were monitored via transabdominal ultrasonography, and offspring were delivered naturally or by cesarean section. DNA isolated from offspring hair plucks was genotyped by polymerase chain reaction (PCR) amplification of the targeted loci and Sanger sequencing of PCR products (following TOPO subcloning when multiple products prevented unambiguous sequence determination). Guide RNA off-target sites were predicted using Benchling.com, amplified from genetically engineered offspring, and Sanger sequenced.

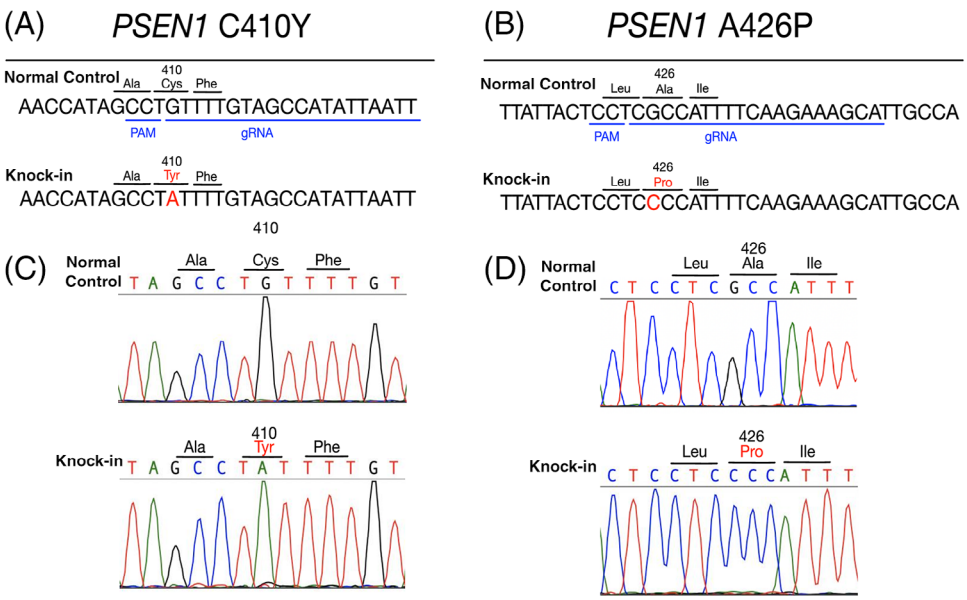

FIGURE 1 Marmoset PSEN1 genetic engineering. (A, B) Partial marmoset PSEN1 normal control (NC) and knock-in (KI) genomic DNA sequences showing relevant amino acids, the protospacer adjacent motif (PAM), and CRISPR gRNA binding sites. The DNA substitutions introduced by CRISPR gene editing and resulting amino acid changes are shown in red in the KI sequence. (C) DNA sequencing chromatograms from normal control and homozygous KI marmosets demonstrating the G to A substitution introduced to change cysteine at 410 to tyrosine. (D) DNA sequencing chromatograms from normal control and subcloned KI amplicon demonstrating the G to C substitution introduced to change alanine 426 to proline.

2.3 | Developmental assessments

Germline offspring (F1) born from the natural mating of a C410Y founder male and a NC female and contemporaneous age- and sex-matched NCs were assessed weekly for developmental trajectories beginning during postnatal week (PNW) 1 through a maximum of 12 weeks (PNW12) or until the developmental milestone was achieved. The developmental trajectory consisted of a battery of assessments that evaluated developmental milestones and were quantified as absence or presence and qualitative response similar to methods previously described.[36–39] Observations included auditory startle response, righting reflex, negative geotaxis, postural control, locomotor activity, hand grasping, visual tracking, hanging, pole climbing, jumping, and depth perception (visual cliff), as well as a series of proprioceptive measures to assess joint/limb positioning (Table S1). Body weight, body length, tail length, and biparietal distance were also measured weekly. A trained analyst blind to genotype scored video recordings anonymized with coded subject IDs.

2.4 | Biomarkers

Blood was collected from the saphenous vein (infants) or the femoral vein (adults) into EDTA-coated tubes and placed onto wet ice, then centrifuged at 4°C for 10 min × >10,000 rpm. Plasma aliquots were stored at −80°C until analysis. MesoScale Discovery (MSD; Rockville, MD, USA) Aβ peptide panel ELISA (4G8; Catalog No. K15199G) was used to evaluate Aβ levels in plasma, while MSD multiplex neurology panel ELISA (Catalog No. K15639S) was used to evaluate plasma glial fibrillary acidic protein (GFAP), neurofilament light chain (NFL), and Tau (total). All plasma biomarker experiments were conducted under blinded conditions and followed the kit recommendations.

2.5 | Brain tissue analysis

2.5.1 | Western blots

Hemispheres without cerebellum from *PSEN1* mutation carrier marmosets and NC controls matched for age at time of death were cold thawed on ice and manually chopped into a homogeneous mixture. The tissue product was weighed and lysed with 8 µL/mg of tissue homogenization buffer, similar to methods previously described.[40] An aliquot of the homogenate was diluted 10× with deionized water and used for Bradford protein quantification according to the manufacturer's protocol (Thermo Fisher Scientific, #23236). For western blots, all samples were diluted with deionized water to a protein concentration of 2 µg/mL. Diluted samples were combined with Laemmli Sample Buffer (Bio-Rad, #1610747) and boiled for 5 min at 95°C. 10 µg of each sample was loaded onto a 4% to 20% gel (Bio-Rad) with a 90-min run time at 120 V. The gel was removed, transferred to the membrane, and incubated on a shaker with blocking buffer for 30 min. The membrane was then incubated with the diluted primary antibody solution (Aβ, APH-1, APP, NCT, PEN-2, PSEN1, PSEN1, and PSEN2; Table S2) on a shaker overnight and rinsed three times for 20 min with TBST.

Secondary antibodies were prepared according to the primary antibody source; rabbit antibodies were incubated with anti-rabbit StarBright 700 (1:3000) and Glyceraldehyde 3-phosphate dehydrogenase (GAPDH) (1:2500) for 1 h, and mouse antibodies were incubated with horseradish peroxidase (HRP) anti-mouse (1:5000) for 1 h. Membranes were rinsed three times in TBST for 5 min. Membranes treated with StarBright 700 secondary antibody were placed directly onto the ChemiDoc Imaging System (Bio-Rad) for visualization; membranes treated with HRP secondary antibody were incubated for 1 min with enhanced chemiluminescence (ECL) Western Blotting Substrate (Thermo Fisher Scientific, #32106) and transferred to the imaging system. Following visualization, HRP-treated membranes were rinsed in TBST, incubated with a GAPDH secondary antibody for 1 h, and then visualized again. Initial western blots were conducted under blind conditions, with the genotype of each sample anonymized until statistical analysis.

2.5.2 | Immunohistochemistry

Immunohistochemical (IHC) protocols with validated antibodies for beta-amyloid (anti-Aβ1-42 rabbit polyclonal antibody (Invitrogen Catalog No. 44-344), and NAB228, a monoclonal antibody for the N-0 terminal of Aβ (Invitrogen Catalog No. 37-4200), microglia (anti-Iba1 goat polyclonal antibody, Abcam Catalog No. ab5076), and NeuN (mouse monoclonal antibody, Millipore Catalog No. MAB377) were used to produce triple immunostaining of marmoset brain tissue. Briefly, after euthanasia, a transcardial perfusion with cold RNase-free PBS was performed, and the right brain hemisphere was placed in 10% NBF (Sigma-Aldrich). The brain hemispheres were then cryoprotected by placing them in 15% and 30% sucrose in 1× PBS solutions. The brains were frozen in isopentane and stored at −80°C. Frozen brains were sectioned to 40 µm thickness using a cryostat (Leica model CM3050 S). Free-floating sections were washed three times for 5 min in 0.1 M PBS and incubated for 30 min in a citrate antigen retrieval buffer (10 mM, pH8.5) that was preheated to 80°C in a water bath. The sections were allowed to cool to room temperature in the antigen retrieval buffer and triple washed for 5 min in 0.1 M PBS. Sections were then incubated in 1% NaBH4 for 30 min in PBS-Triton, triple washed, incubated for 30 min in 0.05 M glycine in PBS-Triton, triple washed, and incubated in blocking solution for 2 h at room temperature. Sections were then incubated at 4°C overnight in the three primary antibodies diluted in antibody solution. Sections were then triple washed in PBS-Triton solution, incubated with secondary antibodies, triple washed in PBS-Triton, mounted onto slides, and visualized using a confocal microscope (Zeiss LSM 900).

2.6 | Statistical analysis

Developmental trajectories were analyzed by two-way repeated measures ANOVA. Longitudinal biomarker data comparing founders and F1 to age- and sex-matched controls were analyzed through a linear mixed-effects model to effectively capture individual and population-mean age-related variations while considering the influence of sex and genetic differences. The linear mixed-effects model equations used for Aβ40, Aβ42, and the Aβ42:40 ratio were, respectively, as follows:

$$A\beta 40^s = \beta_0 + b_0^s + (\beta_1 + b_1^s) \times \text{Age}^s + \beta_2 \times (\text{Age}^s)^2 + \beta_3 \times \text{Sex}^s + \beta_4 \times \text{Genotype}^s + \varepsilon^s$$

$$A\beta 42^s = \beta_0 + b_0^s + (\beta_1 + b_1^s) \times \text{Age}^s + \beta_2 \times \text{Sex}^s + \beta_3 \times \text{Genotype}^s + \varepsilon^s$$

$$A\beta 42:40^s = \beta_0 + b_0^s + (\beta_1 + b_1^s) \times \text{Age}^s + \beta_2 \times \text{Sex}^s + \beta_3 \times \text{Genotype}^s + \varepsilon^s$$

Cross-sectional colony-wide biomarker analysis was analyzed through a linear model to estimate population-mean relationships between the biomarkers and included age, age squared, sex, and genotype as predictors as follows for Aβ40, Aβ42, and Aβ42:40 ratio:

$$A\beta 40^s = \beta_0 + \beta_1 \times \text{Age}^s + \beta_2 \times (\text{Age}^s)^2 + \beta_3 \times \text{Sex}^s + \beta_4 \times \text{Genotype}^s + \varepsilon^s$$

$$A\beta 42^s = \beta_0 + \beta_1 \times \text{Age}^s + \beta_2 \times \text{Sex}^s + \beta_3 \times \text{Genotype}^s + \varepsilon^s$$

$$A\beta 42:40^s = \beta_0 + \beta_1 \times \text{Age}^s + \beta_2 \times \text{Sex}^s + \beta_3 \times \text{Genotype}^s + \varepsilon^s$$

For cross-sectional GFAP analysis, we used a linear mixed model that included age, age squared, sex, and genotype as predictors. The model equation is as follows:

$$\text{GFAP}^s = \beta_0 + \beta_1 \times \text{Age}^s + \beta_2 \times (\text{Age}^s)^2 + \beta_3 \times \text{Sex}^s + \beta_4 \times \text{Genotype}^s + \varepsilon^s.$$

For cross-sectional NFL and tTau, due to skewness the data were subjected to logarithmic transformation with the models calculated as follows:

$$\log(\text{NFL}^s) = \beta_0 + \beta_1 \times \text{Age}^s + \beta_2 \times \text{Sex}^s + \beta_3 \times \text{Genotype}^s + \varepsilon^s$$

$$\log(t\text{Tau}^s) = \beta_0 + \beta_1 \times \text{Age}^s + \varepsilon^s.$$

One-way ANOVA was performed on GFAP, NFL, and tTau data after the subjects were grouped into five categories from "Infant" to "Aged" by their ages with Tukey's test for pairwise comparisons between ages and groups.

Western blots were quantified using ImageJ (National Institute of Health). GAPDH expression was used as a protein control; a ratio was derived for each sample by dividing the antibody of interest's quantification by GAPDH quantification. An average of this ratio was derived for all NC animals and used as an ultimate control. The ratios were then divided by the ultimate control average to estimate a fold increase or decrease in protein from NC controls. The resulting values were analyzed using IBM SPSS Statistics (Version 29). Data were analyzed for each antibody using a one-way ANOVA with genotype as the independent variable and through parametric bivariate correlation of the variables.

3 | RESULTS

3.1 | Generation of PSEN1 mutation carriers

We independently introduced two single base-pair changes into the *PSEN1* gene, one that changes the cysteine 410 codon to tyrosine (C410Y, Figure 1A), and the other changing the alanine 426 codon to proline (A426P, Figure 1B). Figure 1 illustrates the amino acid numbering based on the human gene for ease of comparison. The marmoset-equivalent amino acids are located at positions C409 and A425 in PSEN1, respectively.[41] Figure 1 also illustrates the DNA sequencing chromatograms demonstrating the G to A substitution introduced to change cysteine at 410 to tyrosine (Figure 1C) and the G to C substitution introduced to switch alanine 426 to proline (Figure 1D).

3.1.1 | C410Y mutation carrier founders

Eleven offspring resulted from the transfer of embryos injected with *PSEN1*-C410Y CRISPR reagents (Table 1). Sanger sequencing of PCR amplicons from the targeted region of the *PSEN1* gene revealed genetic alterations in 10 of 11 offspring. Six animals harbored KI mutations; four were viable, and two infants died soon after birth. The four viable KI offspring included one mosaic animal (Subject ID #6) that harbors three alleles in addition to the Y410 KI allele, one animal (Subject ID #5) that is homozygous for the Y410 KI allele, one (Subject ID #4) that is a KI/+1 heterozygote, and one (Subject ID# 217) that is a KI/+2 heterozygote (Table 1). Sequencing 14 of the predicted highest-ranking sites in the four *PSEN1*-C410Y viable founders found no off-target mutations. In addition to these six KI founders, four genetically engineered offspring harbored various insertion/deletion mutations but lacked the C410Y KI mutation (Table 1).

3.1.2 | A426P mutation carrier founders

Six offspring resulted from the transfer of embryos injected with *PSEN1*-A426P CRISPR reagents (Table 1). Two viable singletons (Subject ID #1, Subject ID #200) were delivered at term by cesarean section, and one viable animal (Subject ID #105) was delivered naturally. Twin offspring (Subject ID #8S1; #8S2) and a singleton (Subject ID #35S1) were not viable to term. All six offspring were heterozygous for the A426P allele and a second allele unique to each animal (Table 1). Sequencing seven of the predicted highest-ranking sites in the three *PSEN1*-A426P viable founders found no off-target mutations.

3.2 | Developmental trajectories of germline offspring

Subject ID#4 sired four litters of germline offspring through natural mating with a NC female marmoset (Table 2). Litters were born in February 2022, July 2022, December 2022, and July 2023. The developmental trajectories of the F1 germline offspring carrying the C410Y mutation and their contemporaneous age- and sex-matched NC controls are presented in Figure 2. There were no significant differences in growth or developmental trajectories of PSEN1 F1 marmosets relative to age- and sex-matched NC.

3.3 | Evaluation of biomarkers

Longitudinal assessments of plasma Aβ40, Aβ42, and the Aβ42:40 ratio are presented in Figure 3 and analyzed using a linear mixed-effects model to capture individual and population-mean age-related variations with effects of sex and genotype. *PSEN1* founders exhibited consistent elevations in plasma Aβ42 prior to adulthood, relative to age- and sex-matched controls (Figure 3A). The association between Aβ42 and age and the association between Aβ42 and genotype are statistically significant, as indicated by p values of .015 and 1.6×10^{-4}, respectively. Also, a statistically significant increase in the Aβ42:40 ratio was associated with genotype but not age ($p = 1.5 \times 10^{-8}$; Figure 3C). These differences were present in the absence of differences in plasma Aβ40 in which there was no significant effect of Aβ40 on sex or genotype (Figure 3B). Interestingly, a reduction in plasma Aβ40 with early development was observed in nearly all NC and PSEN1 mutation carrier individuals (Figure 3B). Analysis of Aβ40 revealed statistically significant associations with age ($p = 2.8 \times 10^{-9}$), with nonlinear changes that reach a minimum concentration at 30 months of age, and no effect of sex or genotype. As illustrated in Figure 3D–F, germline offspring (F1) *PSEN1* mutation carriers did not present with elevated levels of plasma Aβ prior to 1 year of age, at which time plasma Aβ42 and the plasma Aβ42:40 ratio were rising relative to age- and sex-matched NC. Analysis of Aβ42 in the F1 revealed a significant effect of genotype ($p = 2.7 \times 10^{-3}$; Figure 3D). There was also a statistically significant effect of both age ($p = 1.2 \times 10^{-3}$) and genotype ($p = 9.3 \times 10^{-3}$) for the Aβ42:40 ratio (Figure 3F). Analysis of Aβ40 in the F1 revealed a statistically significant effect of age ($p = 6.8 \times 10^{-4}$) but not genotype or sex, with Aβ40 reaching a minimum concentration at 12 months of age (Figure 3E). The findings of statistically significant increases in Aβ42 and Aβ42:40 in the F1 were also confirmed by one-way ANOVA with p values of 1.1×10^{-3} and 7.2×10^{-3}, respectively (Figure S1).

To evaluate whether *PSEN1* mutation carriers were presenting with pathological Aβ levels or levels related to normative values across aging marmosets, the colony of $n = 177$ male and female marmosets was evaluated for plasma Aβ levels across ages. As illustrated in Figure 3G–I, Aβ42 and Aβ42:40 ratio levels were elevated in *PSEN1* mutation carriers above the mean across all ages of NCs. Only genotype was found to have significant associations with Aβ42 ($p = 2.1 \times 10^{-5}$) and Aβ42:40 ratio ($p = 1.2 \times 10^{-12}$). There was no significant association between Aβ40 and age, sex, or genotype ($p = .42$). Interestingly, a few NCs also presented with high plasma Aβ42:40 for which whole genome sequencing is in progress. These findings were also confirmed by one-way ANOVA after the subjects were classified

TABLE 1 Summary of PSEN1 founder marmosets created with CRISPR/Cas9 gene editing.

Targeted mutation	Subject ID	Sex	Mosaic	Genotype[a]	DNA sequence	Date of birth	Age at death (days)
C410Y	**REFERENCE**	–	–	**Control KI**	**CCATAGCCTGTTTTGT** **CCATAGCCTATTTTGT**	–	–
C410Y	#6	F	Yes	KI KIΔ1 Δ5 WT	CCATAGCCTATTTTGT CC-TAGCCTATTTTGT CCATAGCCTG−−T CCATAGCCTGTTTTGT	Feb. 5, 2020	806
C410Y	#5	M	No	KI	CCATAGCCTATTTTGT	Feb. 10, 2020	518
C410Y	#4	M	No	KI +1	CCATAGCCTATTTTGT CCATAGCCTGTTTTTGT	Feb. 10, 2020	Alive
C410Y	#217	M	No	KI +2	CCATAGCCTATTTTGT CCATAGCCTGTTTTTTGT	Aug. 2, 2021	485
C410Y	#23S1	ND	No	KI	CCATAGCCTATTTTGT	Feb. 5, 2020	0
C410Y	#44S1	ND	Yes	KI Δ1 +2 Sub1Δ1 Sub1+2	CCATAGCCTATTTTGT CCATAGCCTG-TTTGT CCATAGCCTGTTAATTGT CCATCGCCTG-TTTGT CCATAGTCTGTTTATTGT	Jun. 26, 2020	0
C410Y	#215	M	No	Δ2 +9	CCATAGCCTGT–TGT CCATAGCCTGTTTAATTGTAAGTGT	Jul. 29, 2021	548
C410Y	#216	F	Yes	Multiple indels	Data not shown[b]	Jul. 29, 2021	14
C410Y	#245	M	No	Δ2 Δ12	CCATAGCCTGT–TGT CCA−−−−T	Apr. 12, 2022	515
C410Y	#247	M	No	+2	CCATAGCCTGTTTTTTGT	May 3, 2022	262
C410Y	#17S1	ND	–	WT	CCATAGCCTGTTTTGT	Jun. 29, 2020	0
A426P	**Reference**	–	–	**Control KI**	**TTATTACTCCTCGCCATTTTCAAGAAAGCATTGCCAGC** **TTATTACTCCTCCCCATTTTCAAGAAAGCATTGCCAGC**	–	
A426P	#1	M	No	KI Δ20	TTATTACTCCTCCCCATTTTCAAGAAAGCATTGCCAGC TTATTACTCCTCGCCA−−−−−−−GC	Mar. 28, 2020	708
A426P	#105	F	No	KI indel	TTATTACTCCTCCCCATTTTCAAGAAAGCATTGCCAGC −79 bp indel-CCCATTTTCAAGAAAGCATTGCCAGC	Jul. 22, 2020	438
A426P	#200	F	No	KI Δ7	TTATTACTCCTCCCCATTTTCAAGAAAGCATTGCCAGC TTATTACTCCTC−−-TCAAGAAAGCATTGCCAGC	Jan. 11, 2021	439
A426P	#8S1	ND	No	KI KIΔ2	TTATTACTCCTCCCCATTTTCAAGAAAGCATTGCCAGC T-ATTACTCCTCCCC-TTTTCAAGAAAGCATTGCCAGC	Nov. 15, 2020	0
A426P	#8S2	ND	No	KI KIΔ1	TTATTACTCCTCCCCATTTTCAAGAAAGCATTGCCAGC TTATTACTC-TCCCCATTTTCAAGAAAGCATTGCCAGC	Nov. 15, 2020	0
A426P	#35S1	ND	No	KI KIΔ1	TTATTACTCCTCCCCATTTTCAAGAAAGCATTGCCAGC TTATTACTCCTCC-CATTTTCAAGAAAGCATTGCCAGC	Jan. 8, 2021	0

Note: In the bolded reference DNA sequences, PAM sites are in blue text and knock-in mutations are underlined. In the DNA sequence of individual animals, differences from the control reference sequence are indicated in red text.

[a]Genotypes: KI = knock-in; WT = wild type; Δ = deletion; + = insertion; # = number of basepairs; sub = substitution.

[b]This subject harbored multiple mutant alleles that were never definitively characterized.

into five groups based on age (i.e., Infant [<1 year], Young (1 to 2 years), Adult [2 to 4 years], Aging [5 to 7 years], Aged [>8 years]). For Aβ40, one-way ANOVA revealed no significant effect of age for Aβ40 ($p = .58$ by F-test), Aβ42 ($p = .11$ by F-test), or Aβ42:40 ($p = 0.15$ by F-test), confirming the significance of the PSEN1 genotype on Aβ42 and Aβ42:40.

As presented in Figure 3J–L, the plasma biomarkers GFAP, NFL, and Tau (total) were analyzed cross-sectionally across the population of marmosets in the colony to establish normative values across age. Analysis of GFAP (Figure 3J) revealed a significant non-linear association with age ($p = .0015$), with the estimated mean GFAP level reaching the minimum when the age was around 60 months ($R^2 = 0.13$). There

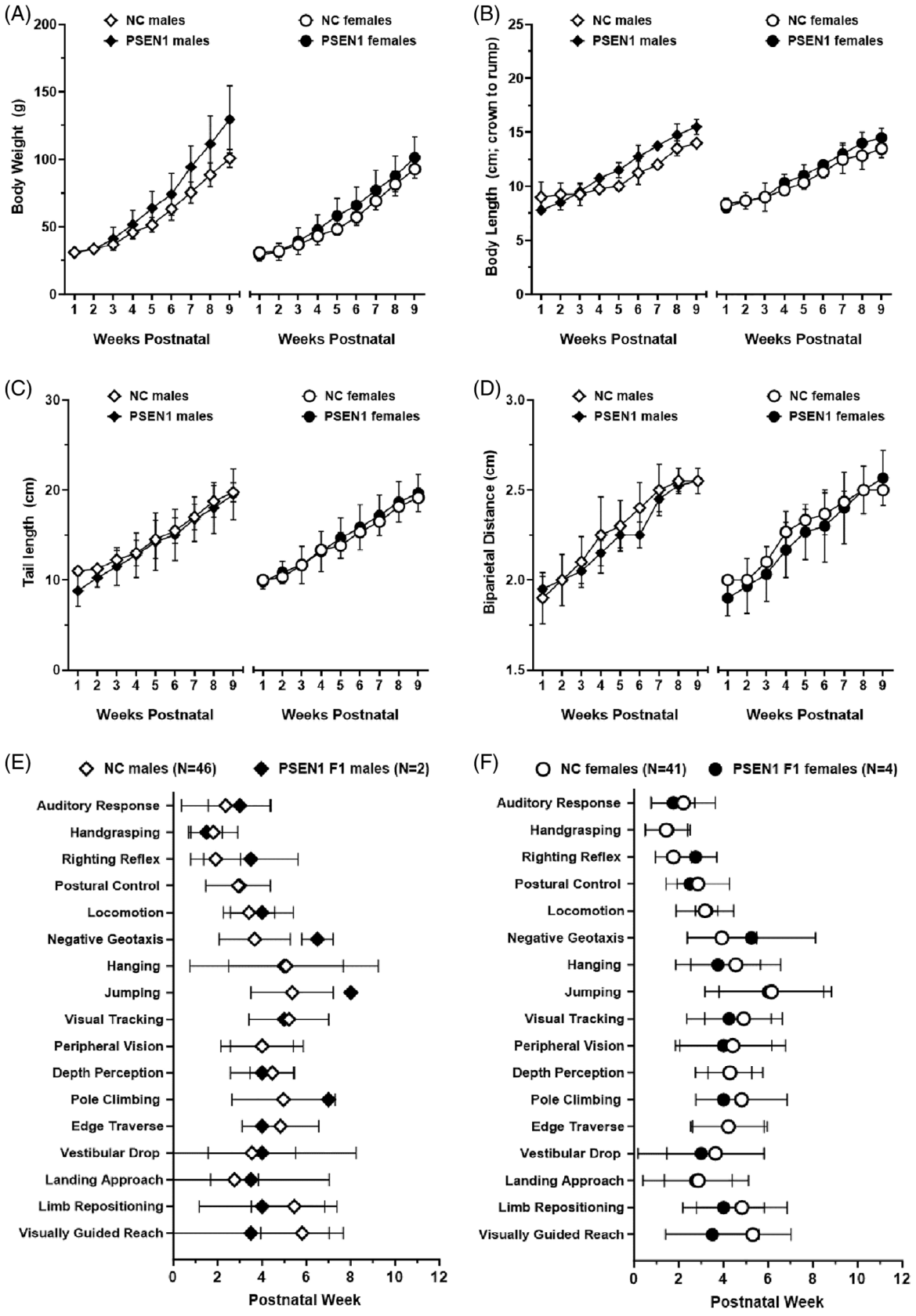

FIGURE 2 Growth and developmental trajectories of PSEN1 F1 germline ($n = 2$ males; $n = 3$ females) and age- and sex-matched non-mutation carriers (NC). Evaluations are conducted once per week beginning from postnatal week (PNW) 1 up to PNW12. (A) body weight; (B) body length (crown to rump); (C) tail length; (D) biparietal distance. Postnatal week at which specific developmental milestones are achieved are presented in (E) males and (F) females relative to age- and sex-matched NC. Demographics for each subject are provided in Table 2, representing litters 2 and 3.

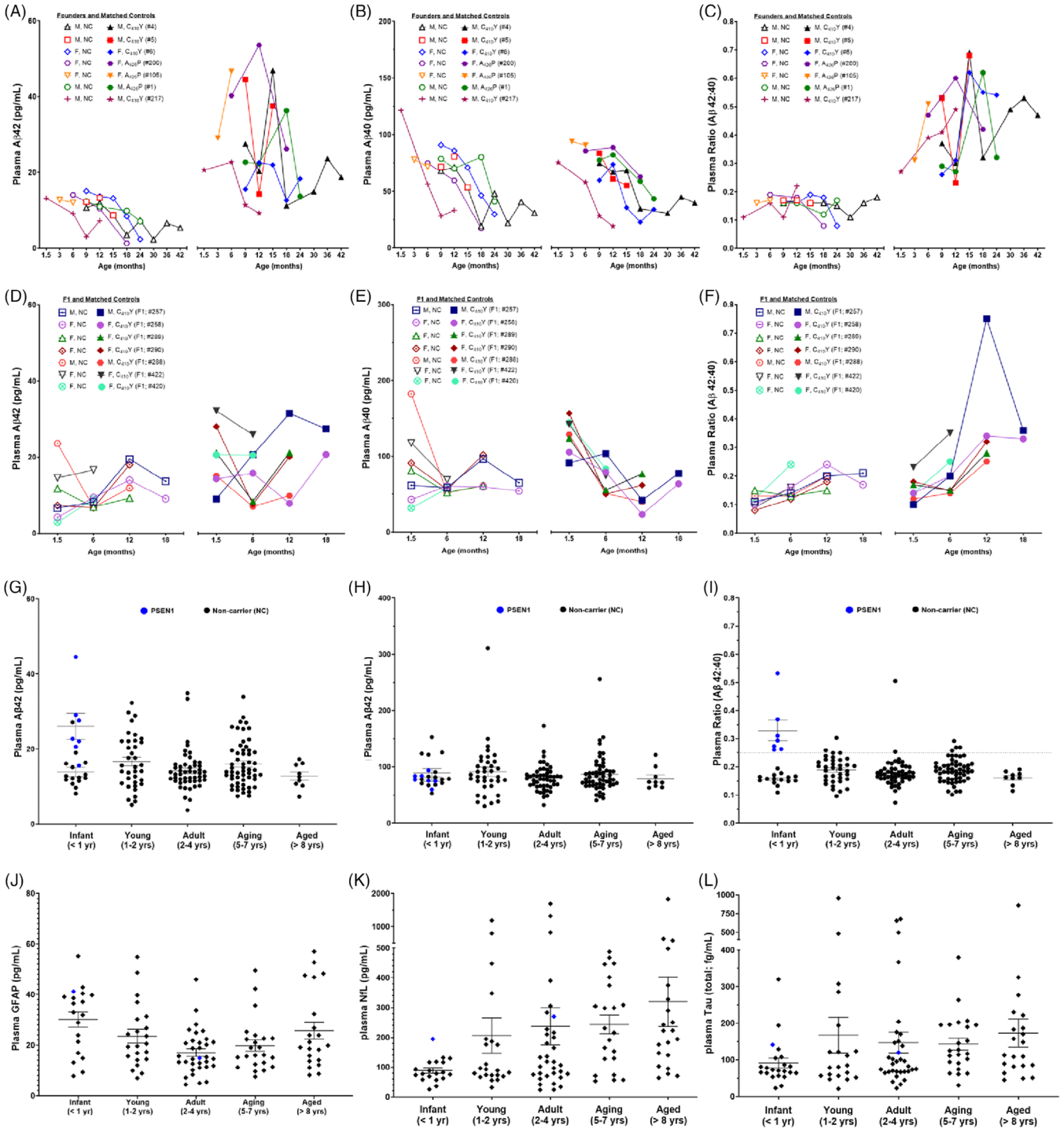

FIGURE 3 Elevations in plasma Aβ levels in PSEN1 mutation carriers. Top panel: longitudinal analysis of plasma from PSEN1 mutation founder marmosets from infancy through adulthood compared to age- and sex-matched contemporaneous non-carrier (NC) controls, (A) plasma Aβ42 (pg/mL); (B) plasma Aβ40 (pg/mL); (C) calculated Aβ42:40 ratio. (D–F) Longitudinal analysis of plasma from infancy to present age for germline offspring (F1) of PSEN1 founder mutation carrier marmosets compared to age- and sex-matched contemporaneous NC controls, (D) plasma Aβ42 (pg/mL); (E) plasma Aβ40 (pg/mL); (F) calculated Aβ42:40 ratio. (G–I) Cross-sectional evaluation of normative values of plasma Aβ levels across a population of aging NC marmosets (black symbols) in comparison to young PSEN1 mutation carrier founder marmosets (blue symbols; subjects from A to C); (G) plasma Aβ42 (pg/mL); (H) plasma Aβ40 (pg/mL); (I) calculated Aβ42:40 ratio. (J–L) Cross-sectional evaluation of normative values of plasma biomarkers (J) GFAP (pg/mL); (K) NFL (pg/mL); and (L) Tau (total, fg/mL). Demographics for each subject are provided in Tables 1 and 2 for Subject ID no. in (A)–(F).

TABLE 2 Summary of F1 offspring derived from natural mating of a C410Y male with a non-carrier female.

Subject ID #	Litter #	Sex	Genotype	Date of birth	Date of death (DD/MM/YY)	Comments
#79S1	1	Female	WT/+1	Feb. 14, 2022	Feb. 14, 2022	Stillborn
#79S2	1	Female	WT/+1	Feb. 14/22	Feb. 15, 2022	Live birth; died on day 1
#79S3	1	Male	WT/+1	Feb. 14, 2022	Feb. 14, 2022	Stillborn
#79S4	1	–	WT/KI	Feb. 14, 2022	Feb. 14, 2022	Underdeveloped fetus
#235	1	Male	WT/KI	Feb. 14, 2022	Feb. 16, 2022	Live birth; died on day 2
#79S5	2	–	WT/+1	Jul. 24, 2022	Jul. 24, 2022	Stillborn
#257	2	Male	WT/KI	Jul. 24, 2022	–	
#258	2	Female	WT/KI	Jul. 24, 2022	–	
#289	3	Female	WT/KI	Dec. 25, 2022	–	
#288	3	Male	WT/+1	Dec. 25, 2022	–	
#290	3	Female	WT/KI	Dec. 25, 2022	–	
#420	4	Female	WT/+1	Jul. 22, 2023	–	
#421	4	Female	WT/+1	Jul. 22, 2023	Jul. 26, 2023	
#422	4	Female	WT/KI	Jul. 22, 2023	–	

was no significant effect of sex ($p = .29$) or genotype ($p = .68$) on GFAP. One-way ANOVA was performed after the subjects were classified into five age categories (i.e., Infant [<1 year], Young [1 to 2 years], Adult [2 to 4 years], Aging [5 to 7 years], Aged [>8 years]). The one-way ANOVA between GFAP and age group had a p value of .002, confirming the significant association found in the linear model. Tukey's test for pairwise comparisons between the age groups revealed that Infant versus Adult group comparison and the Infant versus Aging group comparisons had significant differences in GFAP levels (Figure 3J).

Analysis of NFL (Figure 3K) revealed a significant linear association between age and log-transformed NFL ($p = 3.2 \times 10^{-4}$) with no significant effect of sex ($p = .83$) or genotype ($p = .2$). One-way ANOVA analyzed after the subjects were classified into groups by age confirmed the significant association of age and NFL ($p = .0057$). Tukey's test for pairwise comparisons across age groups revealed significant differences in NFL observed in the Infant versus Aging group comparison and the Infant versus Aged group comparisons (Figure 3K).

As presented in Figure 3L, analysis of plasma Tau (total; tTau) revealed a modest linear association between age and log-transformed tTau ($p = .03$) with no significant association of sex or genotype. One-way ANOVA analyzed after the subjects were classified into groups by age did not demonstrate a significant effect of age ($p = .12$) within the individuals and ages evaluated in the present dataset.

3.4 | Molecular analysis of PSEN1 founders

One founder PSEN1 mutation carrier (male C410Y, Subject ID #4; Table 1) remains healthy at >4 years of age (equivalent to approximately 32 human years) and to date has sired four healthy F1 litters (Table 2). All other founders failed to thrive and required humane euthanasia prior to 2.5 years of age. Analysis of brain tissue and necropsy results from these subjects are described below.

3.4.1 | Necropsy results

Necropsies were performed on marmosets euthanized due to welfare concerns or those found dead, major peripheral organs were collected, and histopathological examinations were performed. A summary of necropsy findings and histopathology are presented in Table S3. Systemic amyloidosis was observed in the liver, kidneys, spleen, and intestines, which was the diffuse deposition of eosinophilic amorphous materials in the tissues with hematoxylin-eosin staining in four of the seven mutation marmosets. The systemic amyloidosis finding is common in aging marmosets and typically reflects general inflammation.[42] Interestingly, in the three cases in which amyloid was not observed, renal findings such as nephritis, nephropathy, and glomerular atrophy, generally observed in older aged marmosets, were present.[43]

3.4.2 | Western blot analysis of PSEN1 and substrates of the gamma–secretase complex

As illustrated in Figure 4 and Figure S2, one-way ANOVA was performed for each primary antibody and corrected for multiple comparisons. Subjects were grouped by genotype: C410Y ($n = 2$), A426P ($n = 2$), and PSEN1+2 carrier ($n = 1$) and compared to NCs ($n = 5$). Mutation carriers demonstrated significantly lower PSEN1 protein levels compared to NCs (Figure 4A; $F[3,3] = 100.033, p < .01, \eta p^2 = 0.990$). Reductions in NCT (Figure 4B) and PEN-2 (Figure 4C) protein were also observed with a significant main effect of genotype for NCT

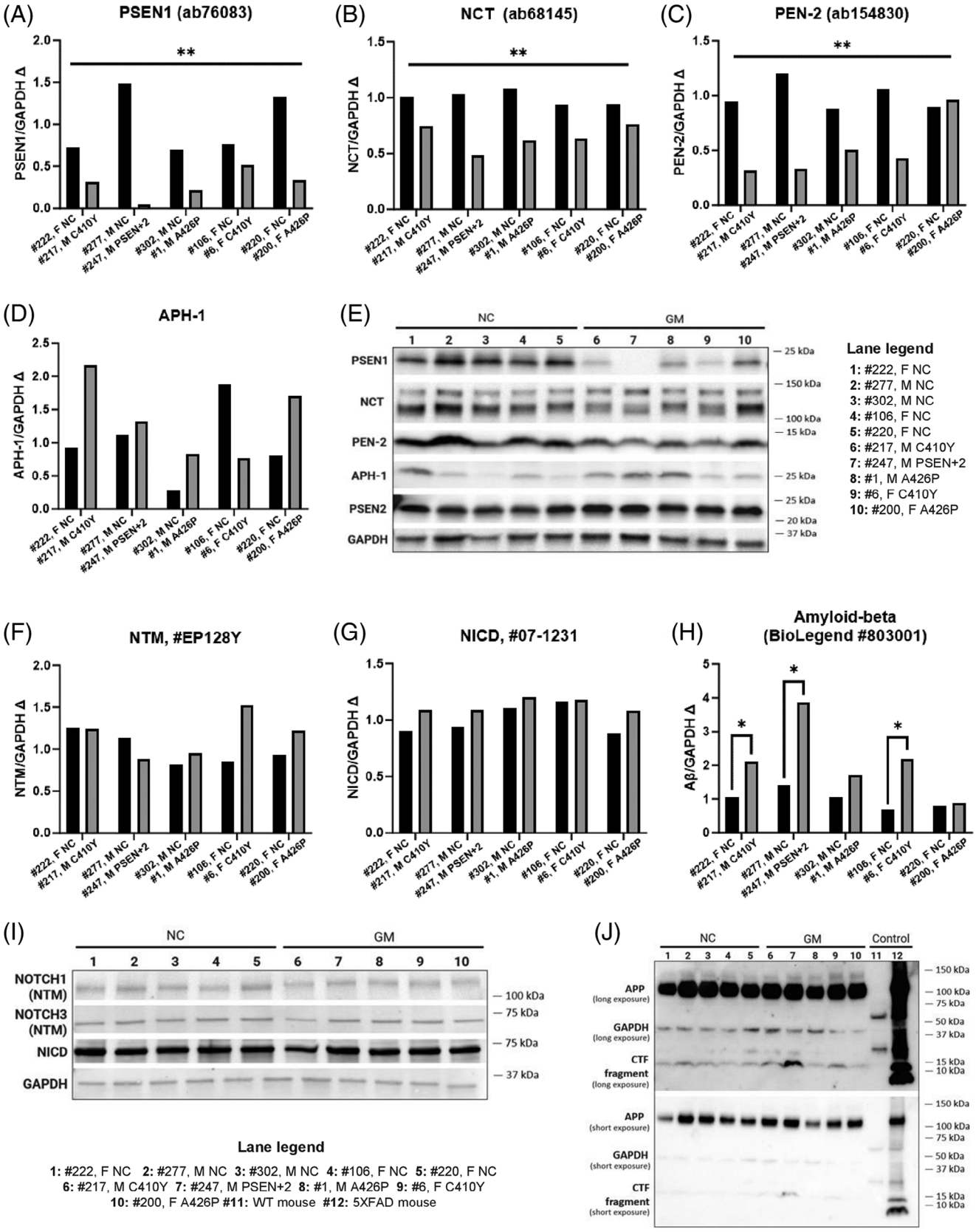

FIGURE 4 Western blot analysis of enzyme–substrate interactions of gamma–secretase complex from cortex of PSEN1 marmoset founders and age-matched non-carrier (NC) control tissues. (A) PSEN1; (B) nicastrin (NCT); (C) PEN-2; (D) APH-1; (E) membrane immunoblots of PSEN1, NCT, PEN-2, APH-1, PSEN2, and GAPDH; (F) NOTCH1 transmembrane domain (NTM); (G) NOTCH intracellular domain (NICD); (H) amyloid beta (Aβ) 6E10; (I) Membrane immunoblots of NTM, NICD, and GAPDH; (J) membrane immunoblots of APP antibody under long exposure (top) and short exposure (bottom), labeled for long-form APP and CTP fragment (Aβ).

(F[3,6] = 21.891, $p < .01$, $\eta p^2 = 0.916$) and PEN-2 (F[3,6] = 10.940, $p < .01$, $\eta p^2 = 0.845$), such that mutation carriers showed a reduction in NCT- and PEN-2/GAPDH ratio compared to NCs. xxxNo differences in APH-1 level were observed between genotypes. NOTCH1 transmembrane (NTM; $p = 0.346$) and intracellular domain (NICD; $p = .122$) proteins also revealed no genotype effects, indicating that despite the introduced PSEN1 mutation, NOTCH1 cleavage appears to remain intact in the founders. Aβ, however, showed a significant effect of genotype (F[3,6] = 23.216, $p < .001$, $\eta p^2 = 0.921$) with C410Y and PSEN1+2 carriers having higher fold Aβ in comparison to NCs (Figure 4H). No main effects of genotype were observed for PSEN2 (F[3,6] = 2.465, $p = .160$), APH-1 (F[3,6] = 0.270, $p = .845$), or soluble APP F[3,6] = 1.376, $p = .337$). A Pearson's bivariate correlation was conducted to examine protein abundance across the PSEN1/γ–secretase complex. A strong positive correlation was observed between NCT and PEN-2 ($r[10] = 0.838$, $p < .01$; NCT and PSEN1 ($r[10] = 0.897$, $p < .001$), and PSEN1 and PEN-2 ($r[10] = 0.718$, $p < .05$). Aβ negatively correlated with NCT ($r[10] = -0.778$, $p < .01$) and PEN-2 ($r[10] = -0.750$, $p < .05$), and while a negative correlation with PSEN1 was trending, the relationship did not meet significance ($r[10] = -0.600$, $p = .067$). Finally, PSEN2 negatively correlated with NCT ($r[10] = -0.632$, $p < .05$) and PEN-2 ($r[10] = -0.835$, $p < .01$), though it did not correlate with PSEN1 ($r[10] = -0.416$, $p = .232$) or PEN-2 ($r[10] = -0.537$, $p = .109$).

3.4.3 | Immunohistochemical analysis

Triple immunostaining of the brain tissue from a founder marmoset homozygous for the PSEN1 C410Y mutation (Subject 5, aged 17 months) are presented in Figure 5. Both intra- and extracellular accumulation of Aβ42 along with neuroinflammation were present across brain regions.

4 | DISCUSSION

The present studies report the successful generation of genetically engineered marmosets carrying KI point mutations in the *PSEN1* gene. Our results are noteworthy in demonstrating that CRISPR/Cas9 can successfully be used in marmosets to insert KI point mutations found in patients with ADAD. The elevated levels of Aβ42 and Aβ42:40 in plasma from adolescence aligns with the early emergence of AD biomarkers reported in children carrying *PSEN1* mutations.[15–17] Importantly, this phenotype is conserved in the germline offspring of the founders, which are the subjects most pertinent for these and future studies.[21]

PSEN1 encodes presenilin 1, a subunit of γ-secretase, the aspartyl protease responsible for Aβ generation.[44,45] *PSEN1* mutations destabilize enzyme–substrate interactions, increasing the relative levels of longer toxic forms of Aβ (>42), resulting in a net effect of overproduction and consequently impaired clearance and disease.[46–48] The present results provide evidence that the *PSEN1* mutations engineered in the marmosets create AD models that follow the time course and trajectory of humans with ADAD.[5–12] Based on these findings, by 4 to 6 years of age in the marmosets, which is the human age equivalent of 32 to 48 years, we predict we will observe the accumulation of Aβ in their brains with positron emission tomography (PET) neuroimaging and possibly early subtle changes in behavior that herald the onset of mild cognitive impairment.[5–12,21] Neuroimaging studies are in progress, including extensive validation studies of ^{11}C-PiB-PET for amyloid and ^{18}F-AV-1451-PET for Tau, for which there have been no published validated protocols to date in marmosets and which we are currently establishing and optimizing.[21] Relatedly, there is no expectation that young PSEN1 marmosets would be expected to demonstrate Tau deposition prior to Aβ deposition, as PSEN1 mutation carriers including individuals with C410Y mutations present with PiB-positive PET well before Tau, which we anticipate we will also observe following a similar trajectory in the C410Y marmosets with aging.[49–51]

While we observed differential trajectories for increasing levels of plasma Aβ in the F1 offspring in comparison to the founders, the aggressive nature of the founder phenotype was somewhat unexpected but may also be a confound of all founder animals being either homozygous KIs or compound heterozygotes that harbor a KI allele in combination with presumptive knockout indel alleles. Humans with ADAD due to PSEN1 C410Y or A426P mutations are always heterozygotes that harbor a normally functioning wild-type (WT) allele in combination with the KI allele. Relatedly, the lack of a WT allele in these founders may have also contributed to early mortality. In mice, homozygous *Psen1* C410Y, L435F, R278I, or complete knockout results in a severe phenotype including embryonic/perinatal mortality.[52] Interestingly, in our studies, one homozygous PSEN1 mutation carrier founder was indistinguishable compared to age- and sex-matched NCs despite high levels of plasma Aβ42 until shortly before the time of death at 17 months of age. Necropsy findings revealed intracellular and extracellular accumulation of Aβ in brain and substantial global amyloidosis, indicative of an accelerated disease trajectory, which may provide insight into the lack of surviving human homozygous C410Y mutation carriers. It is important to point out that not all mutation carrier marmosets presented with systemic amyloidosis at the time of death; therefore, it cannot be concluded that these specific *PSEN1* mutations lead to premature death in marmosets as Founder #4 continues to thrive and produce viable and healthy germline offspring. It can also not be concluded that systemic amyloidosis is a result of these specific mutations, as other common chronic conditions reported in marmosets were observed in both mutation carriers and NCs at necropsy (Table S3).

Although the primary role of the founders is to pass the KI mutation through the germline to subsequently propagate the lineage for further studies, the availability of their brain tissues provided the opportunity to investigate mechanisms and enzyme–substrate interactions as a result of these genetic mutations, albeit with cautious interpretation. For example, relatively few studies thus far have examined the expression of NCT, PEN-2, and APH-1 in response to presenilin mutations despite the importance of the other components of the γ–secretase complex that aid in complex maturation and stabilization for cleavage

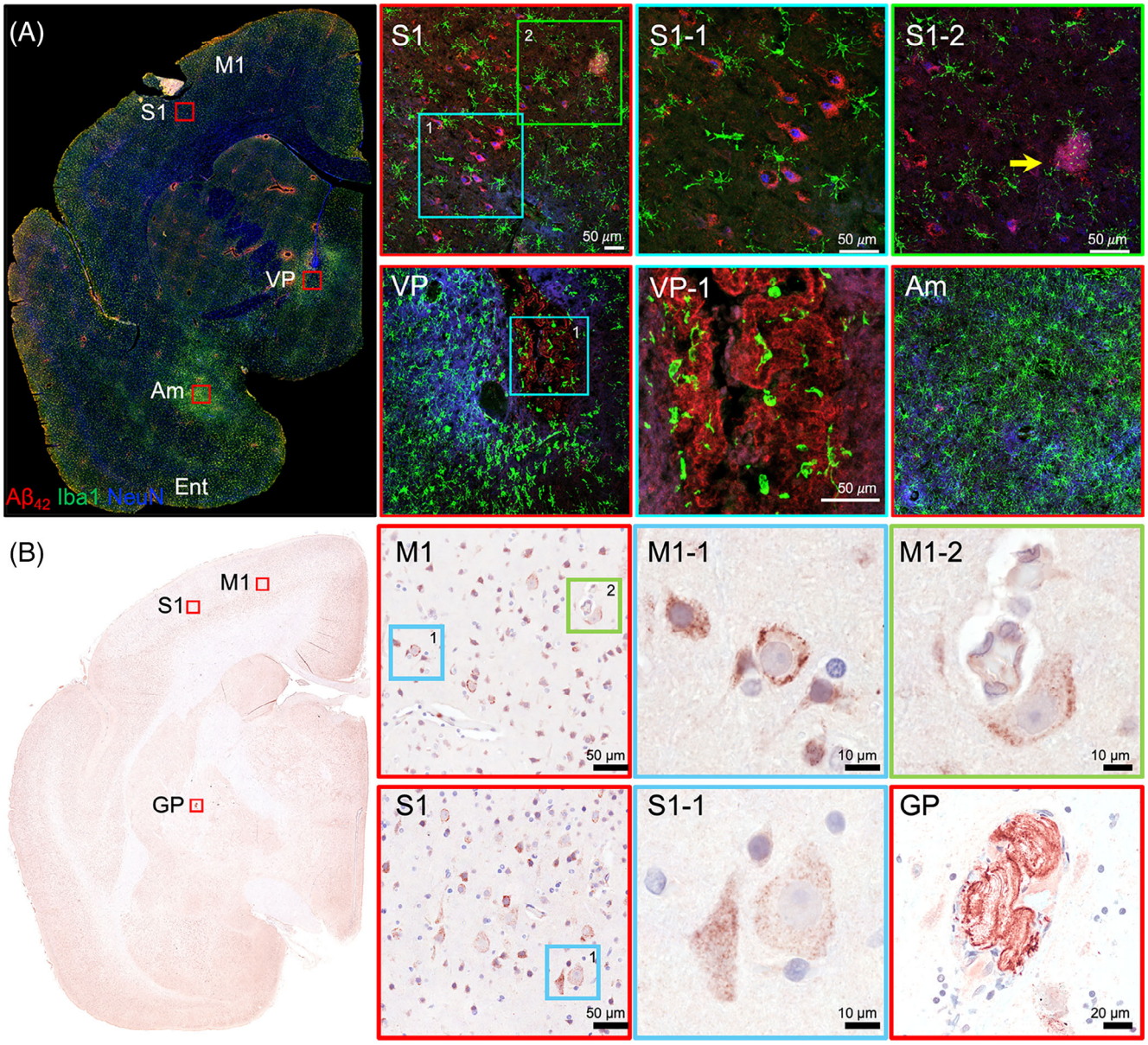

FIGURE 5 (A) Triple immunostaining of a 17-month-old founder marmoset homozygous for PSEN1 C410Y mutation, showing intra- and extracellular accumulation of amyloid beta 42 (Aβ42) (red), along with neuroinflammation (green: anti-Iba1). Cell nuclei were stained with an anti-NeuN antibody (blue). S1: primary somatosensory cortex. M1: primary motor cortex. VP: ventral pallidum. Am: amygdala. Ent: entorhinal cortex. Panel A1: sensorimotor cortex. S1-1: intracellular Aβ. S1-2: extracellular Aβ plaques (arrow). VP: Ventral Pallidum. Panel VP-1: phagocytic microglia (green) within perivascular Aβ accumulation. Am: gliosis in the amygdala (green). (B) Intra- and extracellular Aβ accumulation shown with amyloid precursor protein/amyloid beta (NAB228) antibody in the same animal and coronal plane as in (A). M1 and S1 show two different fields within sensorimotor cortex, and GP shows a field within the globus pallidum region. M1: primary motor cortex, with insets M1-1 and M1-2 showing intracellular Aβ deposits. S1: primary somatosensory cortex, with inset S1-1 showing intracellular Aβ deposits. GP shows extracellular Aβ plaque formation in globus pallidum. Scale bars show magnification for each panel.

efficacy. NCT, specifically, binds to presenilins[53,54] and APH-1[53] to traffic the γ–secretase complex to the plasma membrane. NCT mutations alter the Aβ (38 + 40)/42 ratio,[54–56] suggesting that stability of the γ–secretase complex is an essential component of the APP cleavage pathway in regulating amyloid production. The present results further support the consequence of PSEN1 mutations impacting NCT and PEN-2 activity, which illuminates these substrates as potential targets for early intervention in ADAD. These findings also highlight distinct roles for PSEN1 and PSEN2 in the pathogenesis of ADAD as PSEN1 protein was reduced while PSEN2 was not. This may implicate separate cleavage mechanisms and/or substrate interactions, as multiple studies have suggested that PSEN1 complexes play a more significant role in APP metabolism than PSEN2 complexes.[55,57–62]

In the present studies we observed a pattern of reduced PSEN1, NCT, and PEN-2 expression with intact APH-1, suggesting that the targeted mutations alone or in combination with the indels may

contribute to reduced cleavage efficiency, leading to premature release of longer Aβ peptides. This is supported in our studies by the evidence of higher levels of Aβ42 and Aβ42:40 in PSEN1 founders, which is also conserved in the germline offspring (Figure 3). The resulting impact on Aβ cleavage is observed in C410Y mutant animals, although upstream soluble APP was unaffected, suggesting that α- and β-secretase cleavage is left intact by the mutation, further supporting the correlation between lower PSEN1, NCT, and PEN-2 protein expression and elevated Aβ expression. It is important to note that the present observations, which to our knowledge are the first to explore γ–secretase substrate interactions related to PSEN1 mutations in a NHP model, may contradict previous studies in rodent models, and there are several distinct explanations. First, although the brain tissues from these founder marmosets are of interest to investigate molecular changes prior to disease, the founders are not ideal specimens due to the lack of a normal WT allele, the potential for mosaic expression of the mutation, and the unexpected premature deaths. Second, with respect to data from rodent models, rodents do not naturally present with amyloid accumulation in the brain, likely due to a lack of sequence conservation of APP with humans. Relatedly, PSEN1 mutations engineered into mice have been insufficient in the absence of humanization of, or mutations in, murine APP to fully recapitulate the pathological consequences of AD, and the interaction of targeted mutations with transgenic promoters, which themselves can produce biological and functional artifacts, cannot be ruled out.[63–66] Though the present results from the founder PSEN1 marmosets may also have their limitations, these findings emphasize the importance of studying ADAD mutations early in life prior to disease onset, which will provide greater insights into the root molecular causes of AD.

While this report describes the generation of these marmoset models and initial early phenotypic characterization data, which are already revealing novel insights into molecular changes that precede frank neuropathology as a result of these PSEN1 mutations, comprehensive characterization of these models and their germline lineages is ongoing as part of the MARMO-AD consortium.[21] MARMO-AD is applying the NIA-Alzheimer's Association research framework to characterize the disease trajectory of the marmosets from birth throughout their lifespan.[21,67–69] This includes whole genome sequencing, which is in progress, and may help reveal other genetic factors in our population of outbred marmosets that may contribute to the phenotype of the founder animals and the germline, including polygenic risk factors reported for humans. Although the study of these marmosets is intended as lifespan studies, which limits direct access to brain tissue, we are optimizing protocols to derive neurons and glia annually from fresh fibroblast cultures obtained from skin biopsies and analyzing transcriptomic and proteomic signatures in comparison to AD patients.[21] We will soon conduct PET imaging to assess the onset and progression of Aβ and Tau pathology in these marmosets. These multimodal measures will allow us to further investigate the disease trajectories reported in patients for these PSEN1 mutations.[31] Moreover, while an extensive behavioral and cognitive testing battery is now under way in the germline and their contemporaneous controls, it is unlikely that cognitive decline will be observed until the subjects are aged 4 to 6 years, which is equivalent to the expected age of onset of 32 to 48 when human PSEN1 mutation carriers begin to show cognitive impairment. Relatedly, it is not expected that our PSEN1 marmosets will show significant Tau accumulations, as human PSEN1 mutation carriers present with Tau well after amyloid deposition has been observed,[49–51] and NFTs have only been reported in older (>9 years) marmosets.[70–72]

A recent report described the successful generation of marmosets with *deletion* of exon 9 in the *PSEN1* gene product (*PSEN1*-ΔE9).[73,74] Similar to our results, the *PSEN1*-ΔE9 founders showed overproduction of Aβ42, demonstrating the success of genetic engineering efforts in marmosets to produce an AD-related phenotype, although these marmosets are also not expected to show a cognitive phenotype for several more years.[74] Importantly, given that our goal is to understand the molecular mechanisms that precede cognitive impairment, even in its absence, these marmosets are already recapitulating aspects of the disease trajectory of the human mutation carriers, which emphasizes the importance of these models and their comprehensive characterization throughout their lifespan in order to identify changes that precede frank neuropathology and cognitive decline.

Taken together, results from the present studies indicate that these *PSEN1* mutation carriers display a phenotype of EOAD almost from birth. This observation and the knowledge that can be gained by further study of these animals may provide fundamental insights into the molecular and cellular events that are the root cause of the disease. Critically, these invaluable animal models will provide new avenues of research into how one might intervene to slow or even prevent AD processes.

ACKNOWLEDGMENTS

The authors are grateful to our dedicated marmoset veterinary and husbandry colleagues who provide exceptional care of the marmosets and assistance with these studies. As part of the National Institute on Aging (NIA)-funded Open Science Initiative, all data and protocols are made available through the AD Knowledge Portal (https://adknowledgeportal.synapse.org/Explore/Programs/DetailsPage?Program=MARMO-AD). This work was supported by funding from the National Institutes of Health, NIA grant U19AG074866 and UPMC–ITTC grant IPA 2019 No. 16.

CONFLICT OF INTEREST STATEMENT

Stacey J. Sukoff Rizzo has served as a consultant for Hager Biosciences, GenPrex, Inc., and Sage Therapeutics and holds shares in Momentum Biosciences. Gregory W. Carter has served as a consultant for Astex Pharmaceuticals. Gregg E. Homanics, Jung Eun Park, Lauren Bailey, David J. Schaeffer, Lauren Schaeffer, Tingting Zhang, Annat Haber, Catrina Spruce, Anna Greenwood, Takeshi Murai, Laura Schultz, Lauren Mongeau, Seung-Kwon Ha, Julia Oluoch, Brianne Stein, Sang Ho Choi, Hasi Huhe, Amantha Thathiah, Peter L. Strick, and Afonso C. Silva report no competing interests to declare at the time of submission. Author disclosures are available in the Supporting information.

HUMAN SUBJECT CONSENT

No human subjects were used in these studies, so no consent was necessary.

REFERENCES

1. Goate A, Chartier-Harlin MC, Mullan M, et al. Segregation of a missense mutation in the amyloid precursor protein gene with familial Alzheimer's disease. *Nature*. 1991;349:704-706. doi:10.1038/349704a0
2. Levy-Lahad E, Wasco W, Poorkaj P, et al. Candidate gene for the chromosome 1 familial Alzheimer's disease locus. *Science*. 1995;269(5226):973-977. doi:10.1126/science.7638622
3. Sherrington R, Rogaev E, Liang Y, et al. Cloning of a gene bearing missense mutations in early-onset familial Alzheimer's disease. *Nature*. 1995;375:754-760. doi:10.1038/375754a0
4. Campion D, Dumanchin C, Hannequin D, et al. Early-onset autosomal dominant Alzheimer disease: prevalence, genetic heterogeneity, and mutation spectrum. *Am J Hum Genet*. 1999;65:664-670.
5. Ryman DC, Acosta-Baena N, Aisen PS, et al. Symptom onset in autosomal dominant Alzheimer disease: a systematic review and meta-analysis. *Neurology*. 2014;83:253-260.
6. Perrin RJ, Fagan AM, Holtzman DM. Multimodal techniques for diagnosis and prognosis of Alzheimer's disease. *Nature*. 2009;461(7266):916-922. doi:10.1038/nature08538
7. Jack CR Jr, Knopman DS, Jagust WJ, et al. Hypothetical model of dynamic biomarkers of the Alzheimer's pathological cascade. *Lancet Neurol*. 2010;9(1):119-128. doi:10.1016/S1474-4422(09)70299-6
8. Bateman RJ, Xiong C, Benzinger TL, et al. Clinical and biomarker changes in dominantly inherited Alzheimer's disease. *N Engl J Med*. 2012;367(9):795-804. doi:10.1056/NEJMoa1202753. Epub 2012 Jul 11. Erratum in: N Engl J Med. 2012 Aug 23;367(8):780.
9. Bateman RJ, Benzinger TL, Berry S, et al. The DIAN-TU Next Generation Alzheimer's prevention trial: adaptive design and disease progression model. *Alzheimers Dement*. 2017;13(1):8-19. doi:10.1016/j.jalz.2016.07.005. Epub 2016 Aug 29.
10. Bateman RJ, Aisen PS, De Strooper B, et al. Autosomal-dominant Alzheimer's disease: a review and proposal for the prevention of Alzheimer's disease. *Alzheimers Res Ther*. 2011;3:1.
11. Palmqvist S, Insel PS, Stomrud E, et al. Cerebrospinal fluid and plasma biomarker trajectories with increasing amyloid deposition in Alzheimer's disease. *EMBO Mol Med*. 2019;11(12):e11170. doi:10.15252/emmm.201911170
12. Fuller JT, Cronin-Golomb A, Gatchel JR, et al. Biological and Cognitive Markers of Presenilin1 E280A Autosomal Dominant Alzheimer's Disease: a comprehensive review of the Colombian kindred. *J Prev Alzheimers Dis*. 2019;6(2):112-120. doi:10.14283/jpad.2019.6
13. Karran E, Mercken M, De Strooper B. The amyloid cascade hypothesis for Alzheimer's disease: an appraisal for the development of therapeutics. *Nat Rev Drug Discov*. 2011;10(9):698-712. doi:10.1038/nrd3505
14. Eckerström C, Klasson N, Olsson E, Selnes P, Rolstad S, Wallin A. Similar pattern of atrophy in early- and late-onset Alzheimer's disease. *Alzheimers Dement (Amst)*. 2018;10:253-259. doi:10.1016/j.dadm.2018.02.001. Published 2018 Mar 1.
15. Fox-Fuller JT, Artola A, Chen K, et al. Sex differences in cognitive abilities among children with the autosomal dominant Alzheimer disease presenilin 1 E280A variant from a colombian cohort. *JAMA Netw Open*. 2021;4(8):e2121697. doi:10.1001/jamanetworkopen.2021.21697
16. Quiroz YT, Schultz AP, Chen K, et al. Brain imaging and blood biomarker abnormalities in children with autosomal dominant Alzheimer Disease: a Cross-Sectional Study. *JAMA Neurol*. 2015;72(8):912-919. doi:10.1001/jamaneurol.2015.1099
17. Reiman EM, Quiroz YT, Fleisher AS, et al. Brain imaging and fluid biomarker analysis in young adults at genetic risk for autosomal dominant Alzheimer's disease in the presenilin 1 E280A kindred: a case-control study. *Lancet Neurol*. 2012;11(12):1048-1056. doi:10.1016/S1474-4422(12)70228-4. Epub 2012 Nov 6.
18. De Strooper B, Karran E. The cellular phase of Alzheimer's disease. *Cell*. 2016;164(4):603-615. doi:10.1016/j.cell.2015.12.056
19. Cummings J, Feldman HH, Scheltens P. The "rights" of precision drug development for Alzheimer's disease. *Alz Res Therapy*. 2019;11:76. doi:10.1186/s13195-019-0529-5
20. Cummings J, Zhou Y, Lee G, Zhong K, Fonseca J, Cheng F. Alzheimer's disease drug development pipeline: 2023. *Alzheimers Dement (N Y)*. 2023;9(2):e12385. doi:10.1002/trc2.12385. Erratum in: Alzheimers Dement (N Y). 2023 Jun 28;9(2):e12407.
21. Sukoff Rizzo SJ, Homanics G, Schaeffer DJ, et al. Bridging the rodent to human translational gap: marmosets as model systems for the study of Alzheimer's disease. *Alzheimers Dement (N Y)*. 2023;9(3):e12417. doi:10.1002/trc2.12417
22. Colman RJ. Non-human primates as a model for aging. *Biochim Biophys Acta Mol Basis Dis*. 2018;1864:2733-2741. doi:10.1016/j.bbadis.2017.07.008
23. Perez-Cruz C, Rodriguez-Callejas JD. The common marmoset as a model of neurodegeneration. *Trends Neurosci*. 2023;46(5):394-409. doi:10.1016/j.tins.2023.02.002. Epub ahead of print.
24. Geula C, Nagykery N, Wu CK. Amyloid-beta deposits in the cerebral cortex of the aged common marmoset (*Callithrix jacchus*): incidence and chemical composition. *Acta Neuropathol*. 2002;103(1):48-58. doi:10.1007/s004010100429
25. Maclean CJ, Baker HF, Ridley RM, Mori H. Naturally occurring and experimentally induced beta-amyloid deposits in the brains of marmosets (*Callithrix jacchus*). *J Neural Transm (Vienna)*. 2000;107:799-814. doi:10.1007/s007020070060
26. Palazzi X, Switzer R, George C. Natural occurrence of amyloid-Abeta deposits in the brain of young common marmosets (*Callithrix jacchus*): a morphological and immunohistochemical evaluation. *Vet Pathol*. 2006;43:777-779. doi:10.1354/vp.43-5-777
27. Arnsten AFT, Datta D, Preuss TM. Studies of aging nonhuman primates illuminate the etiology of early-stage Alzheimer's-like neuropathology: an evolutionary perspective. *Am J Primatol*. 2021;83(11):e23254. doi:10.1002/ajp.23254
28. Sharma G, Huo A, Kimura T, et al. Tau isoform expression and phosphorylation in marmoset brains. *J Biol Chem*. 2019;294(30):11433-11444. doi:10.1074/jbc.RA119.008415
29. Rodriguez-Callejas JD, Fuchs E, Perez-Cruz C. Evidence of tau hyperphosphorylation and dystrophic microglia in the common marmoset. *Front Aging Neurosci*. 2016;8:315. doi:10.3389/fnagi.2016.00315
30. Freire-Cobo C, Rothwell ES, Varghese M, et al. Neuronal vulnerability to brain aging and neurodegeneration in cognitively impaired marmoset monkeys (*Callithrix jacchus*). *Neurobiol Aging*. 2023;123:49-62. doi:10.1016/j.neurobiolaging.2022.12.001. Epub 2022 Dec 20.
31. Klunk WE, Price JC, Mathis CA, et al. Amyloid deposition begins in the striatum of presenilin-1 mutation carriers from two unrelated pedigrees. *J Neurosci*. 2007;27(23):6174-6184. doi:10.1523/JNEUROSCI.0730-07.2007
32. National Research Council (US) Committee for the Update of the Guide for the Care and Use of Laboratory Animals. *Guide for the Care and Use of Laboratory Animals*. 8th ed. National Academies Press (US); 2011.
33. Renaud JB, Boix C, Charpentier M, et al. Improved genome editing efficiency and flexibility using modified oligonucleotides with TALEN and CRISPR-Cas9 nucleases. *Cell Rep*. 2016;14:2263-2272. doi:10.1016/j.celrep.2016.02.018
34. Park JE, Zhang XF, Choi SH, Okahara J, Sasaki E, Silva AC. Generation of transgenic marmosets expressing genetically encoded calcium indicators. *Sci Rep*. 2016;6:34931. doi:10.1038/srep34931
35. Takahashi T, Hanazawa K, Inoue T, et al. Birth of healthy offspring following icsi in in vitro-matured common marmoset (*Callithrix*

jacchus) oocytes. *PLoS One*. 2014;9(4):e95560. doi:10.1371/journal.pone.0095560
36. Tardif SD, Layne DG, Cancino L, Smucny DA. Neonatal behavioral scoring of common marmosets (*Callithrix jacchus*): relation to physical condition and survival. *J Med Primatol*. 2002;31(3):147-151. doi:10.1034/j.1600-0684.2002.02005.x
37. Braun K, Schultz-Darken N, Schneider M, Moore CF, Emborg ME. Development of a novel postnatal neurobehavioral scale for evaluation of common marmoset monkeys. *Am J Primatol*. 2015;77(4):401-417. doi:10.1002/ajp.22356
38. Schultz-Darken N, Braun KM, Emborg ME. Neurobehavioral development of common marmoset monkeys. *Dev Psychobiol*. 2016;58(2):141-158. doi:10.1002/dev.21360
39. Wang Y, Fang Q, Gong N. Motor assessment of developing common marmosets. *Neurosci Bull*. 2014;30(3):387-393. doi:10.1007/s12264-013-1395-y
40. Casali BT, Landreth GE. Aβ extraction from murine brain homogenates. *Bio-Protocol*. 2016;6(8):1-4. doi:10.21769/BIOPROTOC.1787
41. Jayakumar V, Ishii H, Seki M, et al. An improved de novo genome assembly of the common marmoset genome yields improved contiguity and increased mapping rates of sequence data. *Bmc Genomics [Electronic Resource]*. 2020;21(Suppl 3):243. doi:10.1186/s12864-020-6657-2
42. Ludlage E, Murphy CL, Davern SM, et al. Systemic AA amyloidosis in the common marmoset. *Vet Pathol*. 2005;42(2):117-124. doi:10.1354/vp.42-2-117
43. Han HJ, Powers SJ, Gabrielson KL. The common marmoset-biomedical research animal model applications and common spontaneous diseases. *Toxicol Pathol*. 2022;50(5):628-637. doi:10.1177/01926233221095449. Epub 2022 May 10.
44. De Strooper B, Iwatsubo T, Wolfe MS. Presenilins and γ-secretase: structure, function, and role in Alzheimer Disease. *Cold Spring Harb Perspect Med*. 2012;2(1):a006304. doi:10.1101/cshperspect.a006304
45. Wolfe MS. Dysfunctional γ-secretase in familial Alzheimer's disease. *Neurochem Res*. 2019;44(1):5-11. doi:10.1007/s11064-018-2511-1. Epub 2018 Apr 4.
46. Chávez-Gutiérrez L, Bammens L, Benilova I, et al. The mechanism of γ-Secretase dysfunction in familial Alzheimer disease. *EMBO J*. 2012;31(10):2261-2274. doi:10.1038/emboj.2012.79. Epub 2012 Apr 13.
47. Selkoe DJ, Hardy J. The amyloid hypothesis of Alzheimer's disease at 25 years. *EMBO Mol Med*. 2016;8(6):595-608. doi:10.15252/emmm.201606210
48. Szaruga M, Munteanu B, Lismont S, et al. Alzheimer's-causing mutations shift Aβ length by destabilizing γ-secretase-Aβn interactions. *Cell*. 2017;170(3):443-456. doi:10.1016/j.cell.2017.07.004.e14
49. Quiroz YT, Sperling RA, Norton DJ, et al. Association between amyloid and tau accumulation in young adults with autosomal dominant Alzheimer disease. *JAMA Neurol*. 2018;75(5):548-556. doi:10.1001/jamaneurol.2017.4907
50. Haleem K, Lippa CF, Smith TW, Kowa H, Wu J, Iwatsubo T. Presenilin-1 C410Y Alzheimer disease plaques contain synaptic proteins. *Am J Alzheimers Dis Other Demen*. 2007;22(2):137-144. doi:10.1177/1533317506298051
51. Moonis M, Swearer JM, Dayaw MPE, et al. Familial Alzheimer disease: decreases in CSF Aβ42 levels precede cognitive decline. *Neurology*. 2005;65(2):323-325.
52. Xia D, Watanabe H, Wu B, et al. Presenilin-1 knockin mice reveal loss-of-function mechanism for familial Alzheimer's disease. *Neuron*. 2015;85(5):967-981. doi:10.1016/j.neuron.2015.02.010
53. Sesele K, Thanopoulou K, Paouri E, Tsefou E, Klinakis A, Georgopoulos S. Conditional inactivation of nicastrin restricts amyloid deposition in an Alzheimer's disease mouse model. *Aging Cell*. 2013;12(6):1032-1040. doi:10.1111/ACEL.12131
54. Yu G, Nishimura M, Arawaka S, et al. Nicastrin modulates presenilin-mediated notch/glp-1 signal transduction and betaAPP processing. *Nature*. 2000;407(6800):48-54. doi:10.1038/35024009
55. Petit D, Fernández SG, Zoltowska KM, et al. Aβ profiles generated by Alzheimer's disease causing PSEN1 variants determine the pathogenicity of the mutation and predict age at disease onset. *Mol Psychiatry*. 2022;27(6):2821-2832. doi:10.1038/s41380-022-01518-6
56. Edbauer D, Winkler E, Haass C, Steiner H. Presenilin and nicastrin regulate each other and determine amyloid beta-peptide production via complex formation. *Proc Nat Acad Sci USA*. 2002;99(13):8666-8671. doi:10.1073/PNAS.132277899
57. Escamilla-Ayala A, Wouters R, Sannerud R, Annaert W. Contribution of the Presenilins in the cell biology, structure and function of γ-secretase. *Semin Cell Dev Biol*. 2020;105:12-26. doi:10.1016/J.SEMCDB.2020.02.005
58. Pintchovski SA, Schenk DB, Basi GS. Evidence that enzyme processivity mediates differential Aβ production by PS1 and PS2. *Curr Alzheimer Res*. 2013;10(1):4-10. doi:10.2174/156720513804871480
59. Watanabe H, Imaizumi K, Cai T, Zhou Z, Tomita T, Okano H. Flexible and accurate substrate processing with distinct presenilin/γ-secretases in human cortical neurons. *eNeuro*. 2021;8(2):1-20. doi:10.1523/ENEURO.0500-20.2021. ENEURO.0500-20.2021.
60. Borgegård T, Gustavsson S, Nilsson C, et al. Alzheimer's disease: presenilin 2-sparing γ-secretase inhibition is a tolerable Aβ peptide-lowering strategy. *J Neurosci*. 2012;32(48):17297-17305. doi:10.1523/JNEUROSCI.1451-12.2012
61. Herreman A, Hartmann D, Annaert W, et al. Presenilin 2 deficiency causes a mild pulmonary phenotype and no changes in amyloid precursor protein processing but enhances the embryonic lethal phenotype of presenilin 1 deficiency. *Proc Natl Acad Sci USA*. 1999;96(21):11872-11877. doi:10.1073/pnas.96.21.11872
62. Sannerud R, Esselens C, Ejsmont P, et al. Restricted Location of PSEN2/γ-secretase determines substrate specificity and generates an intracellular Aβ pool. *Cell*. 2016;166(1):193-208. doi:10.1016/j.cell.2016.05.020. Epub 2016 Jun 9.
63. Dawson TM, Golde TE, Lagier-Tourenne C. Animal models of neurodegenerative diseases. *Nat Neurosci*. 2018;21:1370-1379. doi:10.1038/s41593-018-0236-8
64. Chui DH, Tanahashi H, Ozawa K, et al. Transgenic mice with Alzheimer presenilin 1 mutations show accelerated neurodegeneration without amyloid plaque formation. *Nat Med*. 1999;5(5):560-564. doi:10.1038/8438
65. Jankowsky JL, Zheng H. Practical considerations for choosing a mouse model of Alzheimer's disease. *Mol Neurodegener*. 2017;12(1):89. doi:10.1186/s13024-017-0231-7
66. Sasaguri H, Nilsson P, Hashimoto S, et al. APP mouse models for Alzheimer's disease preclinical studies. *EMBO J*. 2017;36(17):2473-2487. doi:10.15252/embj.201797397. Epub 2017 Aug 1.
67. Jack CR Jr, Bennett DA, Blennow K, et al. NIA-AA Research Framework: toward a biological definition of Alzheimer's disease. *Alzheimers Dement*. 2018;14(4):535-562. doi:10.1016/j.jalz.2018.02.018
68. Murai T, Bailey L, Schultz L, et al. Improving preclinical to clinical translation of cognitive function for aging-related disorders: the utility of comprehensive touchscreen testing batteries in common marmosets. *Cogn Affect Behav Neurosci*. 2024. doi:10.3758/s13415-023-01144-x. Epub ahead of print. PMID: 38200282.
69. Cummings J. The National Institute on Aging-Alzheimer's Association Framework on Alzheimer's disease: application to clinical trials. *Alzheimers Dement*. 2019;15:172-178. doi:10.1016/j.jalz.2018.05.006
70. Freire-Cobo C, Rothwell RS, Varghese M, et al. Neuronal vulnerability to brain aging and neurodegeneration in cognitively impaired marmoset monkeys (*Callithrix jacchus*). *Neurobiol Aging*. 2023;123:49-62. doi:10.1016/j.neurobiolaging.2022.12.001

71. Rodriguez-Callejas JD, Fuchs E, Perez-Cruz C. Evidence of tau hyperphosphorylation and dystrophic microglia in the common marmoset. *Front Aging Neurosci*. 2016;8:315. doi:10.3389/fnagi.2016.00315. Erratum in: Front Aging Neurosci. 2017 Feb 21;9:32.
72. Rizzo SJS, Choi S-H, Huhe H, et al. Differential brain expression of 3R and 4R Tau isoforms in aging wild-type and young genetically engineered PSEN1 mutant marmosets. *Alzheimer's Dement*. 2022;18:e069206. doi:10.1002/alz.069206
73. Sato K, Sasaguri H, Kumita W, et al. A non-human primate model of familial Alzheimer's disease. *bioRxiv*. preprint doi:10.1101/2020.08.24.264259
74. Sasaguri H, Hashimoto S, Watamura N, et al. Recent advances in the modeling of Alzheimer's disease. *Front Neurosci*. 2022;16:807473. doi:10.3389/fnins.2022.807473

SUPPORTING INFORMATION

Additional supporting information can be found online in the Supporting Information section at the end of this article.

How to cite this article: Homanics GE, Park JE, Bailey L, et al. Early molecular events of autosomal-dominant Alzheimer's disease in marmosets with PSEN1 mutations. *Alzheimer's Dement*. 2024;1-17. https://doi.org/10.1002/alz.13806